Double resonant Raman spectra in graphene and graphite: A two-dimensional explanation of the Raman amplitude

Rohit Narula and Stephanie Reich
Department of Materials Science and Engineering, Massachusetts Institute of Technology, Cambridge, Massachusetts 02139, USA
Fachbereich Physik, Freie Universität Berlin, 14195 Berlin, Germany
(Received 9 July 2008; published 24 October 2008)

We report calculated Raman spectra of the D and 2D modes in graphene and graphite. Evaluating the Raman amplitude in the two-dimensional Brillouin zone, we reproduce the splitting of the modes when going from single-layer graphene to graphite. The energy dependence of the D mode in graphene is 24%–32% smaller than in graphite. We discuss the intensity of the D line and show that the double resonant phonons originate from the low-symmetry parts of the Brillouin zone.

DOI: 10.1103/PhysRevB.78.165422 PACS number(s): 78.30.Fs, 81.05.Uw, 63.20.D−

I. INTRODUCTION

The Raman spectra of graphene and related materials such as graphite and carbon nanotubes provide a probe into their fundamental physics, vibrational band structure, electron-phonon coupling, etc.[1–4] They are also promising as a cheap and quick means of fingerprinting sp^2 carbon in a manufacturing environment. The defect-induced D mode and its overtone the 2D mode (historically known as G' and sometimes D^*) are ideal candidates owing to their characteristic structure and excitation-energy dependence for different variants of sp^2 bonded carbon.[1,3] For example, the 2D mode is a single peak in graphene but splits into a multipeak structure when the graphene layers stack to form graphite.[3,5] While this behavior has been explained qualitatively, a detailed theoretical model is missing. Also lacking is knowledge about the origin of the experimentally observed phonons within the hexagonal Brillouin zone. This would be crucial for mapping the phonon dispersion from Raman experiments.[4–6]

In this paper we used a full two-dimensional integration within second-order perturbation theory to calculate the D and 2D modes for graphene and graphite for excitation energies in the visible range. Using solely the tight-binding $\pi-\pi^*$ electronic bands and the experimentally obtained graphite TO phonon dispersion[6] as input parameters, we achieved close agreement with experimental results. Beside the contribution of electron scattering, we also included the complementary hole scattering processes that are no longer redundant owing to the asymmetry of the valence and conduction bands as captured by the nonzero parameter $s_0 = 0.07$ in our tight-binding model. We show that the dominant peaks in the D mode spectra originate from phonons between the K and M points of the Brillouin zone. Finally, we assign individual peaks to their respective scattering processes that are uniquely identified beforehand.

II. METHOD

We follow the established theory of double resonant Raman scattering to describe the D and 2D modes of sp^2 carbon.[1,7,8] Within this framework, the calculation of the Raman spectrum requires a two-dimensional integration over the graphene Brillouin zone. This integration was omitted in most previous publications; (with the exception of Kurti *et al.*[9]) instead the phonons were restricted to high-symmetry lines or the double resonant process was evaluated graphically. Here we work with the full Raman amplitude (also referred to as the Raman matrix element in the literature) [from Eq. (7.24) of Ref. 10] for deriving the D mode

$$K_{2f,10}(q_1,q_2) = \sum_{k_1,k_2} \frac{M_{eR,\rho} M_{e\text{-defect}} M_{ep} M_{eR,\rho}}{[E_1 - E_a^e(k_1,k_2) - i\gamma][E_1 - \omega_{\text{ph}} - E_b^e(k_1,k_2) - i\gamma][E_1 - \omega_{\text{ph}} - E_a^e(k_1,k_2) - i\gamma]}$$
$$+ \sum_{k_1,k_2} \frac{M_{eR,\rho} M_{e\text{-defect}} M_{ep} M_{eR,\rho}}{[E_1 - E_a^e(k_1,k_2) - i\gamma][E_1 - E_d^e(k_1,k_2) - i\gamma][E_1 - \omega_{\text{ph}} - E_a^e(k_1,k_2) - i\gamma]}$$
$$+ \text{corresponding terms for scattering of holes}, \quad (1)$$

where $E_a^e(k_1,k_2)=E_c^e(k_1,k_2)-E_v^e(k_1,k_2)$, $E_b^e(k_1,k_2,q_1,q_2)=E_c^e(k_1-q_1,k_2-q_2)-E_v^e(k_1,k_2)$, and $E_d^e(k_1,k_2,q_1,q_2)=E_c^e(k_1+q_1,k_2+q_2)-E_v^e(k_1,k_2)$. $E_c^e(k_1,k_2)$ and $E_v^e(k_1,k_2)$ are the energies of the conduction and valence bands, respectively, and k_1 and k_2 are the two-dimensional components of the electronic wave vector. ω_{ph} denotes the phonon energy and is a function of q_1 and q_2: the two-dimensional components of the phonon wave vector. γ is the broadening parameter and its value was set to 0.1 eV. E_1 is the excitation laser energy. For the D mode calculation we considered both time orders, i.e., phonon-assisted scattering followed by elastic defect scattering which corresponds to the first term in the summation of Eq. (1) and vice versa. The matrix elements in the above expression—$M_{eR,\rho}$, $M_{e\text{-defect}}$, M_{ep}, $M_{eR,\rho}$ corresponding to the photonic excitation of an electron-hole pair, elastic defect scattering, phonon-assisted scattering, and electron-hole recombination, respectively—were taken to be constant. An expression corresponding to Eq. (1) was used to obtain the Raman amplitude for the 2D mode.

For graphene we considered the well-known first-nearest-neighbor tight-binding expression for the electronic band structure [Eq. (3.20) of Ref. 10] with experimentally fit constants: $\gamma_0=-2.84$ eV and $s_0=0.07$. The electronic dispersion for graphite was taken from Ref. 11 with recommended values of the tight-binding parameters found therein. Both band structures around the K point are presented in Figs. 1(a) and 1(b) clearly showing the splitting of the bands in the case of graphite. Since the dominant contribution to the D and 2D modes comes from the scattering across the K point in the electronic dispersion, we focused the integration of Eq. (1) on a region around the K point with an energy cutoff of about 6 eV for incident laser energies in the visible spectrum.

The D mode contribution associated with electron scattering and its first time-order term in the Raman amplitude of Eq. (1) is shown in Fig. 1(a) for graphene. This single-scattering process corresponds to four scattering processes in graphite [Fig. 1(b)] because of the splitting of the electronic bands.

For the phonon dispersion we fit a third-nearest-neighbor tight-binding expression to the experimental data obtained for graphite via inelastic x-ray scattering.[6] The fit around the K point is shown in Fig. 2. We also considered *ab initio* calculations as input parameters but found that they underestimated the slope of the TO branch around the K point.

In evaluating the Raman amplitude in Eq. (1) we exploited the symmetry of the tight-binding expressions of graphene and graphite that reflect their hexagonal structure, thereby restricting our calculation to only 1/6th of a sector around the K point. The summation in the expression for $K_{2f,10}$ was carried out for $84\times84=7056$ (k_1,k_2) points in the electronic dispersion. The resulting expression was then evaluated for $34\times21=784$ (q_1,q_2) points by again focusing around the K point of the TO phonon. Continuous spectra were generated by multiplying each resulting value with a normalized Gaussian of appropriate half width. We carefully verified that our symmetry-based restrictions did not introduce spurious results by comparing with several calculations evaluating the entire Brillouin zone.

The dominance of the TO branch of the phonon dispersion to the D mode spectra of graphene has been discussed

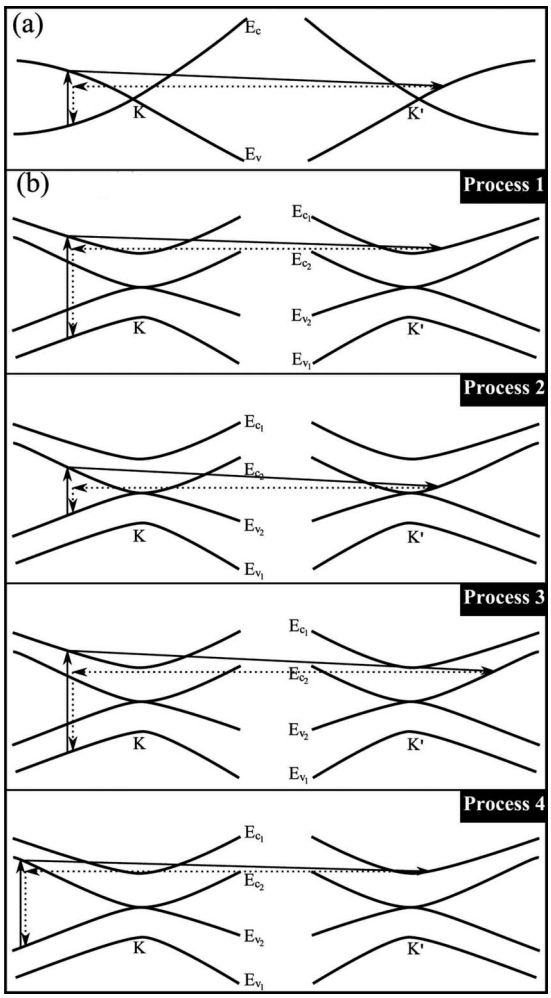

FIG. 1. The $\pi-\pi^*$ electronic band structure of (a) graphene and (b) graphite around the K point showing the individual electron-scattering processes corresponding to the first time-order D mode. The dark and dotted lines represent the resonant and nonresonant transitions, respectively.

based on symmetry-based arguments earlier.[12] These arguments may be applied in an identical manner to the scattering processes 1 and 2 in graphite [Fig. 1(b)], which invoke the T_1 phonon band. For processes 3 and 4, however, the situation is slightly different. Processes 3 and 4 require phonon-assisted scattering across the Γ point [see Fig. 1(b)] which occurs between states of different symmetry ($T_2\rightarrow T_4$ and $T_4\rightarrow T_2$ for processes 3 and 4, respectively). This requires a phonon

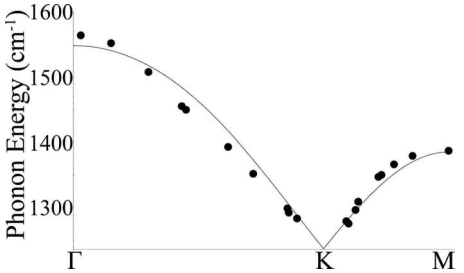

FIG. 2. The experimentally obtained TO phonon dispersion of graphite fit to the data from Ref. 6.

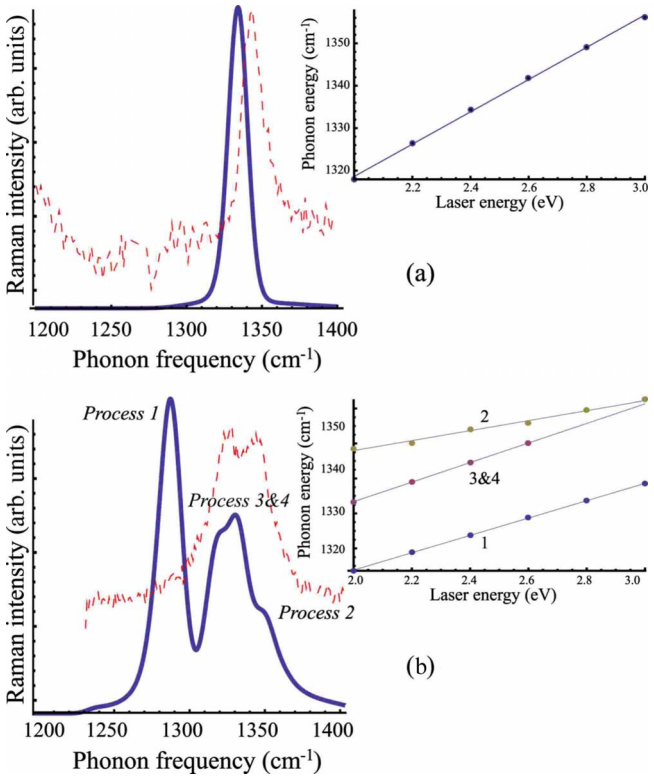

FIG. 3. (Color online) The calculated D mode Raman spectra of (a) graphene and (b) graphite (solid lines) for laser energy 2.4 eV versus the experimental spectra at 514 nm (dashed lines) [data from Ferrari *et al.* (Ref. 3)]. The insets show the excitation-energy dependence of the position of the D mode peak corresponding to the electron-scattering processes shown in Fig. 1. The excitation-energy dependence for graphene is 38 cm^{-1}/eV. While for scattering processes 1, 3&4 and 2 in graphite, they are 50, 56, and 29 cm^{-1}/eV, respectively.

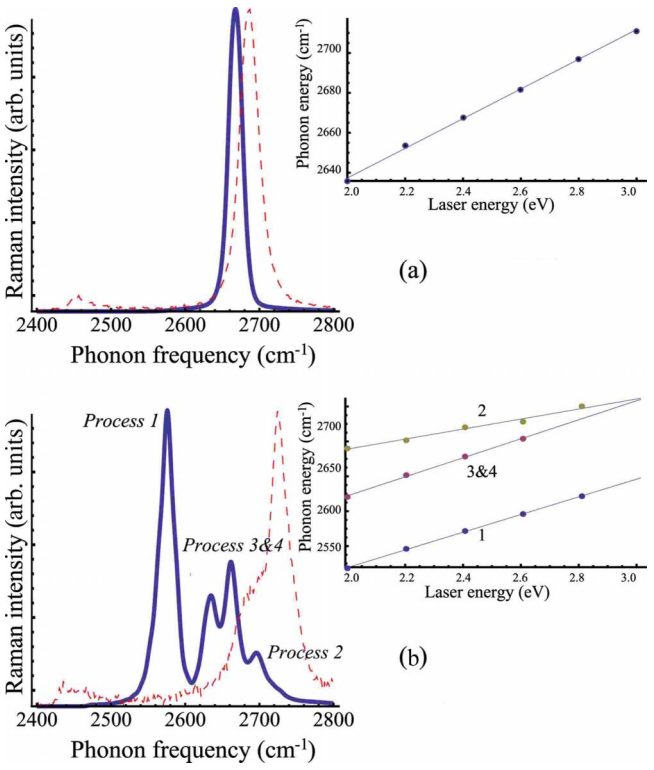

FIG. 4. (Color online) The calculated 2D mode Raman spectra of (a) graphene and (b) graphite (solid lines) for laser energy 2.4 eV versus the experimental spectra (dashed lines) at 514 nm [data from Ferrari *et al.* (Ref. 3)]. The insets show the excitation-energy dependence of the position of the 2D mode peak corresponding to the electron-scattering processes shown in Fig. 1. The excitation-energy dependence for graphene is 74 cm^{-1}/eV. While for scattering processes 1, 3&4 and 2 in graphite, they are 103, 111, and 58 cm^{-1}/eV, respectively.

belonging to the T_3 representation. Just like the splitting of the bands in the case of the electronic dispersion in graphite, the TO phonon branch also splits into two bands possessing symmetries T_1 and T_3.[3,13] The phonon frequencies corresponding to the T_3 branch are not known experimentally. *Ab initio* calculations predicted a splitting of only 1.5 cm^{-1} (Ref. 3), and we therefore modeled the T_1 and T_3 bands as a single phonon branch.

III. RESULTS AND DISCUSSION

In Fig. 3(a) we compare our calculated D mode Raman spectrum of graphene with the experimental results of Ferrari *et al.*[3] The calculated spectrum exhibits the same single peak structure as observed experimentally. The absolute position of the D mode peak also matches very closely. Our calculations predict an almost linear excitation-energy dependence of the D mode with a slope of 38 cm^{-1}/eV [inset of Fig. 3(a)]. The single D peak splits into three in our calculation of graphite shown in Fig. 3(b). This compares very well to the experimental peak [dashed line in Fig. 3(b)], which appears to be a superposition of smaller peaks. The splitting of the D mode in graphite arises from the splitting of the electronic band structure [Fig. 1(b)], as noted by Ferrari *et al.*[3] The individual peaks in Fig. 3(b) are labeled by their respective contributing electron-scattering processes of Fig. 1(b). The excitation-energy dependence for the D mode in graphite is 50 cm^{-1}/eV for the scattering process 1, 56 cm^{-1}/eV for processes 3&4, and 29 cm^{-1}/eV for process 2. This is consistent with experiments that report shifts of 44–51 cm^{-1}/eV.[13–15]

The above discussion follows analogously for the 2D mode spectra that are shown for graphene and graphite in Figs. 4(a) and 4(b), respectively. The shift of the 2D peak with excitation energy is doubled compared to the D mode, as expected. For graphene, the shift is calculated to be 74 cm^{-1}/eV, while for processes 1, 3&4 and 2 in graphite we get 103, 111, and 58 cm^{-1}/eV, respectively.

We further analyzed our results by restricting the summation in Eq. (1) to the different time orders. Defect scattering followed by phonon scattering results in a contribution to the Raman peak that is two orders of magnitude smaller than the first time order: phonon is first and defect is second, although between them their respective Raman peaks occur at almost the same phonon energy. From the experimental spectra we observe that the peak due to the scattering process 2 forms a shoulder of the broad overall peak. Our calculations predict a

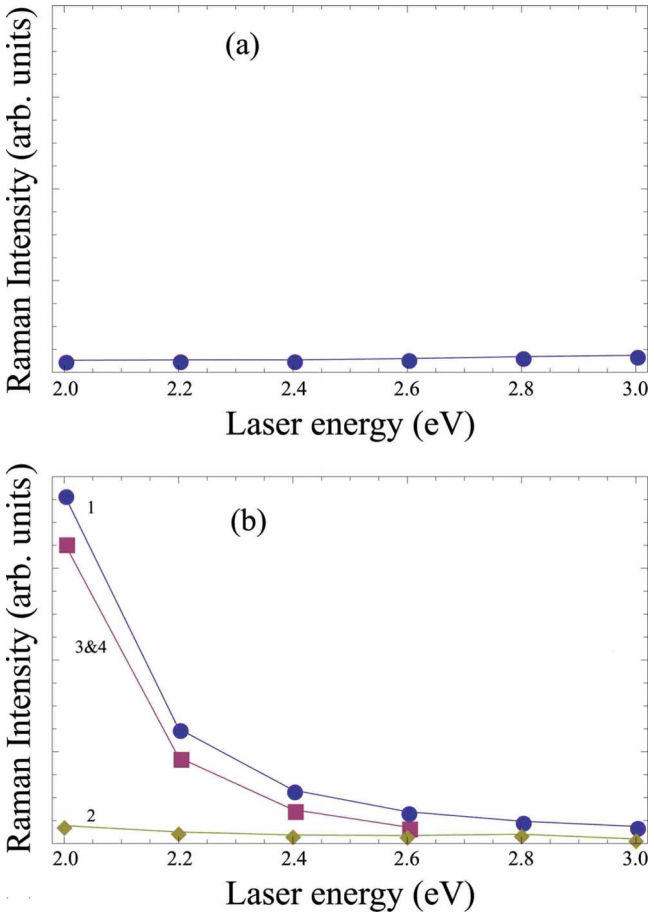

FIG. 5. (Color online) Excitation-energy dependence for peak intensity of the D mode in (a) graphene and (b) graphite. The individual scattering processes in graphite are shown by filled circles for process 1, squares for processes 3&4 and diamonds for process 2. Compare with Fig. 1(b).

much slower shift of its peak position with laser excitation energy and much lower peak intensity of peak 2 relative to peaks 1 and 3&4 at lower energies. The essential features of the experimental spectra viz, threefold splitting of the experimental peak, excitation energy, and peak intensity dependence of peaks 1, 2 and 3&4 as well as the slower shift of peak 2 with laser energy can be reproduced by considering solely the electron scattering which is tantamount to the assumption of symmetric valence and conduction bands. The inclusion of the complementary hole scattering processes results in a slight downshift (~ 1 cm^{-1}) and broadening of the total calculated spectra.

The D and 2D modes of graphite increases in intensity with decreasing laser energy as reported by Pocsik *et al.*[13] and Wang *et al.*[14] We show the calculated peak intensity for graphene in Fig. 5(a) and graphite in Fig. 5(b). Our calculations predict that graphene is expected to have approximately constant peak intensity in the visible range of energies. Comparable to experiment, graphite shows diminishing peak intensity with increasing excitation laser energy for peaks associated with processes 1 and 3&4. The peak associated with process 2, however, remains constant in intensity. The resonant transition associated with the phonon-assisted scattering

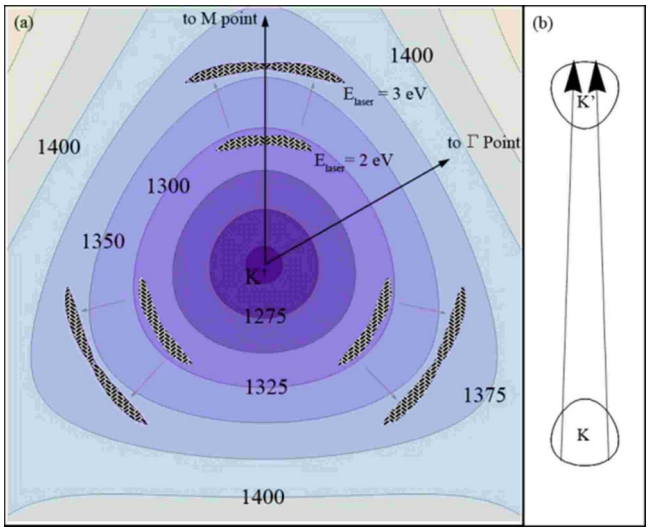

FIG. 6. (Color online) (a) The overlay of $|K_{2f,10}|^2$ (hatched region) due to electron scattering on the phonon dispersion of graphite for the D mode of graphene for laser energies 2.00 and 3.00 eV. (b) The dominant phonon-assisted transitions responsible for the D mode of graphene.

across the Γ point occurs between regions around the K and K' points that are much closer to the Van Hove singularity associated with the K points for the case of processes 1 and 3&4 in graphite than for graphene and process 2 in graphite. This coupled with the mutual interference of the terms within the summation of the Raman amplitude results in $K_{2f,10}(E_1)$, exhibiting a singularity close to the excitation energies of interest (2–3 eV) for the case of processes 1 and 3&4 in graphite. As these energies lie on the shoulder of this singularity, we observe diminishing peak intensity with excitation energy. For graphene and process 2 in graphite the excitation energies of interest lie very far away from the singularity and in a region that is relatively flat, and therefore, show a flat excitation-energy dependence for their respective peak intensities.

In their original paper Thomsen and Reich[1] suggested the use of double resonant Raman scattering for probing the phonon dispersion. Saito *et al.*[4] applied this concept to fit the phonon dispersion of graphite. Similar attempts were made in Ref. 8. The use of Raman data as a probe for the vibrational dispersion in sp^2 carbon materials requires knowledge of the wave vectors of the dominant phonons. The wave vectors are often deduced from the electronic dispersion by connecting energy contours with the same energy (sometimes the phonon energy is explicitly included). This procedure may lead to spurious results because of interference effects; see Maultzsch *et al.*[12] and Martin and Falicov[7] for the discussion.

Figure 6(a) shows the most resonant part of the Raman amplitude (hatched regions) for excitation energies of 2 and 3 eV superimposed on the contour plot of the TO phonon dispersion around the K point (in blue). Surprisingly, the dominant resonant contribution comes from a small region around the K point in the K-M direction. The contribution from the K-Γ direction vanishes by interference. As expected the dominant resonant annulus translates radially outward on

increasing the laser excitation energy, thus, resulting in the near-linear shift of the D mode peak as shown in the inset of Fig. 3(a) for laser energies between 2 and 3 eV.

The position of the most resonant contributions to the Raman amplitude within the graphene Brillouin zone affects the calculated frequency shift of the D mode with laser excitation energy. Restricting the phonon wave vectors to the *K*-*M* high-symmetry line the laser frequency dependence decreases by 5% although the difference is small. The difference originates from the trigonal distortion of the graphene phonon dispersion [see Fig. 6(a)].

Another open question is "which are the most resonant *electronic* wave vectors in the double resonant process?" Earlier calculations[9] argued that the highest intensity maximum in the D mode spectra can be associated with the phonon wave vector transition between the lowest curvature portions around the *K* and *K'* points of the electronic dispersion in the *K*-*M* direction. Our calculations show that instead the dominant contribution comes from a curved to a flat transition as shown in Fig. 6(b), thus, also emphasizing the small contribution from the *K*-Γ direction.

Figure 7 shows a schematic of the overlay of $|K_{2f,10}|^2$ for excitation energy of 2 eV on the contour plot of the phonon dispersion, indicating the regions that make the most resonant contributions for the case of the D mode in graphite. These are labeled according to the electron-scattering processes in Fig. 1(b). In similar fashion to graphene the dominant regions translate outward on increasing the excitation laser energy resulting in the near-linear shift of the D mode peak with changing excitation laser energy. Again the *K*-Γ phonon wave vectors do not contribute to the D mode spectrum.

After submission of our manuscript we became aware of *ab initio* calculations of the graphene phonon dispersion based on the GW formalism.[16] The new calculations are in much better agreement with inelastic x-ray scattering data than previous attempts. The results of Lazzeri *et al.*[16] verified our choice of using the empirical expression fit to experiment as a phonon dispersion as opposed to existing first-principles calculations.

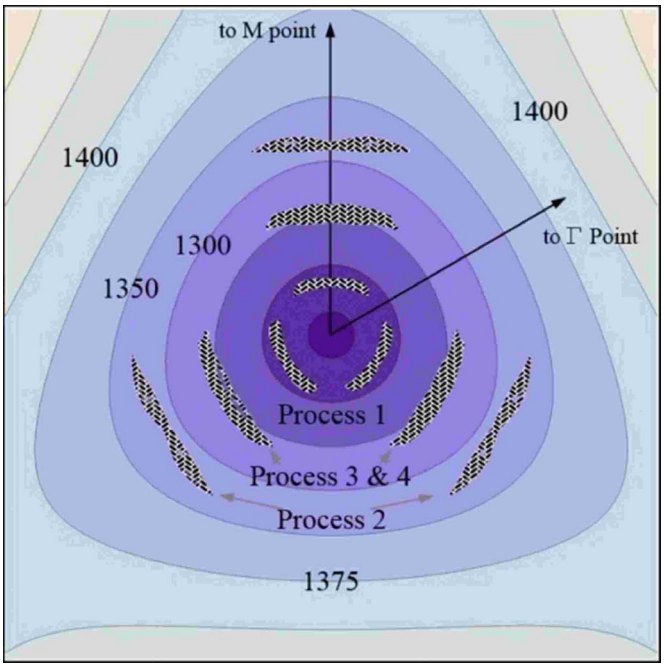

FIG. 7. (Color online) The overlay of the dominant region of $|K_{2f,10}|^2$ (hatched region) due to electron scattering on the phonon dispersion of graphite for the D mode of graphite with laser energy 2.00 eV corresponding to the individual processes identified in Fig. 1(b).

IV. CONCLUSIONS

In summary, we have shown that the characteristics of the D and the 2D modes of graphene and graphite follow from double resonant Raman scattering. Our calculated frequency shifts for the graphite D mode (~50 cm^{-1}/eV) agrees well with experiment (44–51 cm^{-1}/eV); we also reproduced the increasing D mode (2D mode) intensity with decreasing laser energy. For graphene we predict a smaller D mode slope (38 cm^{-1}/eV) and a constant scattering intensity which would be interesting to test experimentally. The strongest contributions to the D and 2D spectra originate from phonons close to the *K*-*M* line. Double resonant scattering between *K* and Γ vanishes by interference. This has to be kept in mind while mapping the phonon-dispersion curves from the double resonant Raman spectrum.

[1] C. Thomsen and S. Reich, Phys. Rev. Lett. **85**, 5214 (2000).
[2] S. Piscanec, M. Lazzeri, F. Mauri, A. C. Ferrari, and J. Robertson, Phys. Rev. Lett. **93**, 185503 (2004).
[3] A. C. Ferrari, J. C. Meyer, V. Scardaci, C. Casiraghi, M. Lazzeri, F. Mauri, S. Piscanec, D. Jiang, K. S. Novoselov, S. Roth, and A. K. Geim, Phys. Rev. Lett. **97**, 187401 (2006).
[4] R. Saito, A. Jorio, A. G. Souza Filho, G. Dresselhaus, M. S. Dresselhaus, and M. A. Pimenta, Phys. Rev. Lett. **88**, 027401 (2001).
[5] D. Graf, F. Molitor, K. Ensslin, C. Stampfer, A. Jungen, C. Hierold, and L. Wirtz, Nano Lett. **7**, 238 (2007).
[6] J. Maultzsch, S. Reich, C. Thomsen, H. Requardt, and P. Ordejón, Phys. Rev. Lett. **92**, 075501 (2004).
[7] R. M. Martin and L. M. Falicov, in *Light Scattering in Solids I*, Topics in Applied Physics Vol. 8, edited by M. Cardona (Springer, Berlin, 1983), p. 79.
[8] S. Reich and C. Thomsen, Philos. Trans. R. Soc. London, Ser. A **362**, 2271 (2004).
[9] J. Kürti, V. Zólyomi, A. Grüneis, and H. Kuzmany, Phys. Rev. B **65**, 165433 (2002).
[10] S. Reich, C. Thomsen, and J. Maultzsch, *Carbon Nanotubes: Basic Concepts and Physical Properties* (Wiley, Weinheim, UK, 2004), p. 128.
[11] B. Partoens and F. M. Peeters, Phys. Rev. B **74**, 075404 (2006).

[12] J. Maultzsch, S. Reich, and C. Thomsen, Phys. Rev. B **70**, 155403 (2004).
[13] I. Pocsik, M. Hundhausen, M. Koos, and L. Ley, J. Non-Cryst. Solids **227-230**, 1083 (1998).
[14] Y. Wang, D. C. Alsmeyer, and R. L. McCreery, Chem. Mater. **2**, 557 (1990).
[15] M. J. Matthews, M. A. Pimenta, G. Dresselhaus, M. S. Dresselhaus, and M. Endo, Phys. Rev. B **59**, R6585 (1999).
[16] M. Lazzeri, C. Attaccalite, L. Wirtz, and F. Mauri, Phys. Rev. B **78**, 081406 (2008).